Journal of Materials and Electronic Devices 1 (2024) 7-12

Structural and Electrochemical Insights into $Pt_{65}Cu_{35}$ Alloy for Enhanced HER Performance

Mustafa Zeki Kurt[1],

[1]Department of Physics, Faculty of Art and Sciences, Cukurova University, Adana, Turkey

This study presents a comprehensive structural and electrochemical characterization of $Pt_{65}Cu_{35}$ alloy nanoparticles (NPs) for their application in the hydrogen evolution reaction (HER). X-ray diffraction method have been used to determine structural properties and revealed a well-defined crystal structure corresponding to the face-centered-cubic (fcc) Pt_3Cu_1 alloy phase, evidenced by characteristic Miller indices as the (111), (200), (220), (311), and (222) planes. Further examination yielded a uniform lattice constants of 3.923 Å, indicating a homogeneous crystal lattice. Assessment of crystallite size, 2.9 nm, and microstrain, 3.85%, underscored the influence of PtCu alloy formation on structural defects and grain boundaries within the NPs. The stoichiometric calculation via energy-dispersive X-ray spectroscopy confirmed Pt and Cu ratio with a percentage of 65 and 35 in the structure and scanning electron microscope showed a spherical morphology attributed to the influence of polyvinylpyrrolidone molecules during synthesis. Moreover, electrochemical investigations revealed promising HER catalytic performance, with cyclic voltammetry (CV) analyses demonstrating Pt-H formation followed by H_2 gas formation. Linear sweep voltammetry (LSV) analysis confirmed a maximum current density of 1.52 mA cm^{-2} was achieved at -0.37 V, indicating high catalytic activity. Furthermore, CV curves recorded over 500 cycles elucidated cyclic behavior, with a current density of 3.04 mA cm^{-2} gradually decreasing over subsequent cycles before stabilizing beyond the 100th cycle. These findings underscore the exceptional electrocatalytic performance of $Pt_{65}Cu_{35}$ catalysts, highlighting their potential for various electrochemical applications. Further research avenues may focus on elucidating underlying mechanisms governing cyclic behavior to optimize catalyst design for enhanced performance and durability.

Keywords: *PtCu nanoparticle, Polyol method, SEM-EDS, XRD, Hydrogen evolution reaction*

Submission Date: 03 December 2023
Acceptance Date: 05 March 2024

**Corresponding author: mzkurt@cu.edu.tr*

1. Introduction

In meeting the escalating global demand for sustainable energy alternatives, electrocatalysis emerges as a remarkably efficient method. Addressing the escalating global energy demands, this technology generates environmentally sustainable, renewable, and uncontaminated energy sources [1]. The electrocatalysis of the water-splitting process assumes a crucial role in the production of high-purity hydrogen and oxygen gases, offering an efficient means not only for electricity generation but also for mitigating the greenhouse effect [2]. Despite the established protocols for hydrogen gas production, the imperative to advance environmentally friendly and cost-effective technologies for large-scale implementation persists [3].

The hydrogen evolution reaction (HER) holds significant importance in electrochemistry, occurring in both acidic and

alkaline environments, albeit with notable differences. In acidic electrolyte, the reaction occurs faster than alkaline electrolyte, approximately two orders of magnitude, resulting in higher current densities [4]. Water and hydronium ions serve as primary reactants in alkaline and acidic electrolytes, respectively. Despite extensive study, the precise mechanism of the HER remains elusive. There are two main theories proposed to explain the HER in alkaline media: water dissociation theory and hydrogen binding theory, with the latter emphasizing the pivotal role of pH in altering the OH^- concentration, thereby impacting the kinetics of the reaction [5].

Platinum group metals (PGMs), renowned for their exceptional electrochemical activities, are often utilized despite their high cost [6, 7]. To mitigate this, PGMs are frequently alloyed with transition group metals, such as Cu, Co, Ni, Fe, etc., to enhance activity and reduce production costs [8-10]. Incorporating metals such as Cu into the alloy modifies the electronic structure at the surface, the distance between Pt-Pt atoms, and the surface roughness, ultimately improving catalytic efficiency. Specifically, Pt-Cu bimetallic nanostructures have shown promising catalytic performances across various applications due to their cost-effectiveness and favorable electronic structure modifications [4, 11-13]. The preparation of catalytic materials with precise control over shape and size is vital for practical applications, with solution-based chemical routes such as the polyol method offering a robust approach for synthesizing Pt and Cu-based nanoparticles (NPs) with desired characteristics. Despite numerous studies on model surfaces, direct investigations of PtCu alloy NPs remain limited, highlighting a gap in current research that warrants further exploration.

In this study, PtCu alloy NPs were successfully synthesized via a modified polyol process and then subjected to thorough characterization to determine their structural and catalytic properties for the HER. Structural analysis techniques, including X-ray diffraction (XRD) and scanning electron microscopy (SEM), were employed to determine the morphology, size, and crystal structure of the PtCu NPs. Additionally, the catalytic performance of the synthesized nanoparticles for the HER was evaluated using cyclic voltammetry (CV) and linear sweep voltammetry (LSV) techniques. By correlating the structural features of the PtCu NPs with their catalytic activities, insights into the relationship between NP characteristics and HER performance were gained, offering valuable implications for the design and optimization of efficient electrocatalysts for renewable energy applications.

2. Experimental

2.1. Synthesis of $Pt_{65}Cu_{35}$ NPs

For the synthesis process of $Pt_{65}Cu_{35}$ NPs, 0.085 g Cu(II)acetate (Sigma-Aldrich ≥98.0%) and 0.343 g Pt(II)acetylacetonate (Sigma-Aldrich ≥97.0%) precursors were dissolved in 30 ml dimethylformamide (ISOLAB ≥99.8%) and subjected to sonication, ensuring the formation of a homogeneous mixture. Subsequently, this mixture poured in 35 ml of the primary reducing agent, ethylene glycol (ISOLAB ≥99.8%), was introduced into a three-necked flask and vigorously stirred for 15 minutes. To stabilize the pH, 0.805 g of sodium hydroxide (ISOLAB ≥98%) and as a surface coating agent, 0.107 g of polyvinylpyrrolidone (Sigma-Aldrich, Mav: 40000) were added into the mixture at room temperature. The sealed system underwent a gradual temperature increase, reaching 120 °C under Ar gas flow and 1.218 g of sodium borohydride (Sigma-Aldrich ≥98%), acting as a secondary reducing agent, was slowly introduced into the system for further reduction of Pt and Cu precursors. Then the mixture temperature increased to 155 °C and annealed for 1 hour for the final product. When the mixture temperature reach to 40 °C, Ar gas flow shut down and the system opened and 4 ml of the solution was mixed with 6 ml of ethanol and centrifuge at 9000 rpm for 10 minutes.

2.2.Electrode Preparation and Electrochemical Performance Test of PtCu NPs

Conducting electrochemical analyses involved the use of a Gamry 1010E potentiostat. For the electrochemical measurements, three-electrode system used: the reference electrode was a Ag/AgCl in 3 M KCl, while the counter electrode comprised a 6 x 6 mm^2 platinum plate (99.95% pure). To create catalytic inks, 4 mg of PtCu NPs was mixed with 28 µl EG, 20 µl DMF and 8 µl 5% Nafion. After subjecting this mixture to 10 minutes of sonication and 1 minutes of vortexing, 1 mg of PtCu NPs ink was deposited onto the surface of a pristine carbon electrode with a diameter of 5 mm. The coated electrode underwent a 24-hour drying process in a furnace. Cyclic voltammetry (CV) measurements were executed in a 1 M KOH alkaline solution within the potential range from -1.2 V to 1.2 V (vs. Ag/AgCl). For linear sweep voltammetry (LSV) measurements, the potential was swept between 0 and -1.6 V vs. Ag/AgCl) at a scan rate of 25 mV s^{-1}, using a step size of 2 mV at room temperature.

3. Results and Discussion

3.1. Structural Properties of PtCu NPs

The NPs' crystal structures underwent examination utilizing a PANalytical XRD system featuring Cu-Kα radiation (λ= 1.54 Å). XRD data revealed to the structural properties of $Pt_{65}Cu_{35}$ NPs were collected within the range of 2θ= 20°-110°. Fig. 1(a) illustrates the XRD data of $Pt_{65}Cu_{35}$ NPs. The observed peaks at 2θ=39.8°, 45.9°, 67.3°, 81.1°, and 87.1° are indicative of the (111), (200), (220), (311), and (222) planes, respectively. These peaks correspond to the characteristic of the face-centered-cubic (fcc) Pt_3Cu_1 alloy phase [4]. The $d_{(111)}$-space value were determined to be 2.26 Å and the lattice constant was found to be a=3.923 Å [14]. PtCu NPs devoid of any impurity and other oxide phases in the XRD patterns predominantly exhibited the Pt_3Cu_1 phase. Assessment of crystallite size, 2.9 nm, and microstrain, 3.85%, involved calculating values derived from the full width at half maximum. The PtCu alloy may exhibit structural defects and grain formations within the structure, with vacancies and grain boundaries emerging as influential factors in the catalytic process. On the other hand, the prevalence of the (111) facets in PtCu-based NPs typically correlates with heightened HER activities.

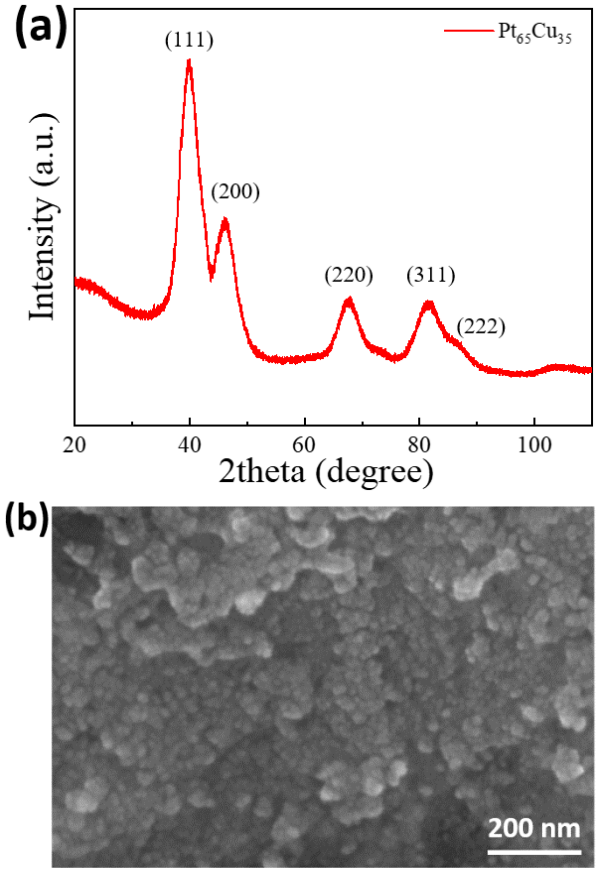

Fig.1. (a) XRD patterns of $Pt_{65}Cu_{35}$ NPs showing Miller indices and (b) SEM image.

Characterization of the PtCu NPs was undertaken utilizing scanning electron microscopy-energy-dispersive X-ray spectroscopy (SEM-EDS, FEI Quanta 650) techniques to reveal the morphology and composition. The SEM image in Fig. 1(b) illustrates the spherical formation of PtCu NPs, a consequence of the influence exerted by PVP molecules, guiding the NPs towards a spherical nanostructure [15]. Fig. 2(a and b) shows EDS performance location on the selected image of $Pt_{65}Cu_{35}$ NPs surface and EDS spectrum and elemental percentage for Pt, Cu and O elements, respectively. EDS spectra delineated elemental analysis, featuring peaks corresponding to Pt and Cu elements based on their energy levels. The relative intensities of Cu and Pt in the EDS data concurred closely with the XRD spectra, with higher Pt content observed in the $Pt_{65}Cu_{35}$ structure, aligning closely with the Pt peaks [13]. Using the percentage of 26.98 and 14.24 for Pt and Cu, respectively, the stoichiometry of PtCu NPs found to be 65% Pt and 35% Cu in the structure. As seen in Fig. 2(b), M and L shells of Pt observed at low and at high energies, respectively. Similarly, L and K shells of Cu observed at low and at high energies, respectively.

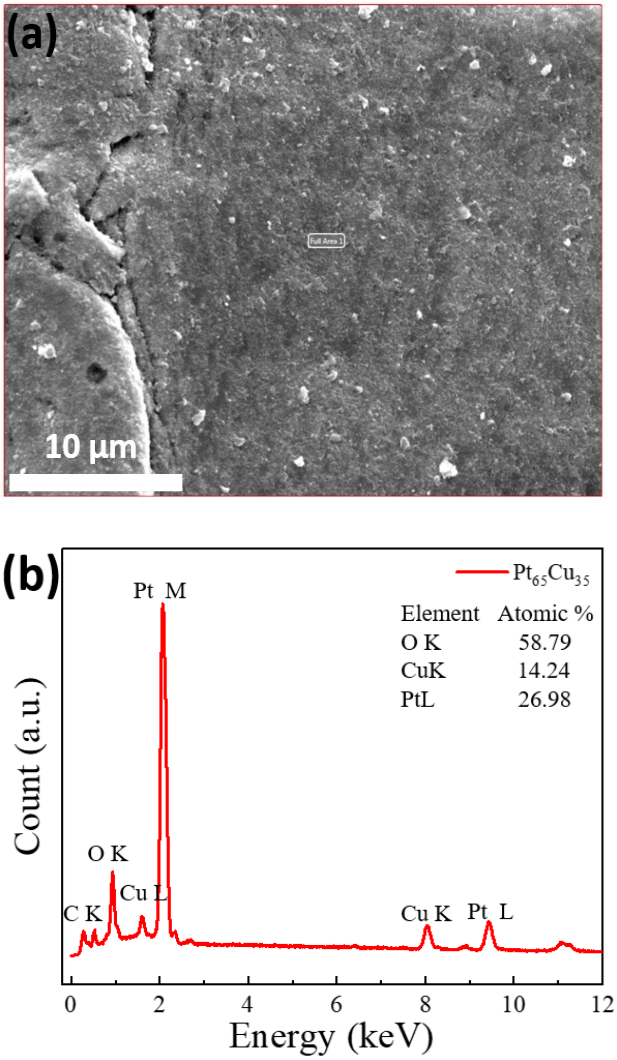

Fig. 2. (a) EDS performance location on the selected image of $Pt_{65}Cu_{35}$ NPs surface. (b) EDS spectrum and the percentage of Pt, Cu, O, and C elements.

3.2. Electrocatalytic Properties of $Pt_{65}Cu_{35}$ NPs

Evaluation of the electrocatalytic performance of the $Pt_{65}Cu_{35}$ catalyst for HER was conducted at ambient temperature. In Fig. 3(a), CV curves of $Pt_{65}Cu_{35}$ catalysts were captured at a scan rate of 50 mV s^{-1} in a 1 M KOH electrolyte, revealing Pt-H formation in the potential range of -0.18 V and -0.77 V (vs. Ag/AgCl) and followed by H_2 gas production. Notably, the maximum current density reached 1.52 mA cm^{-2} at a voltage of -0.37 V. Additionally, Fig. 3(b) illustrates the LSV curve of $Pt_{65}Cu_{35}$ catalysts, recorded with a scan rate of 50 mV s^{-1} in a 1 M KOH electrolyte at room temperature, showcasing an onset potential recorded at -0.87 V [14].

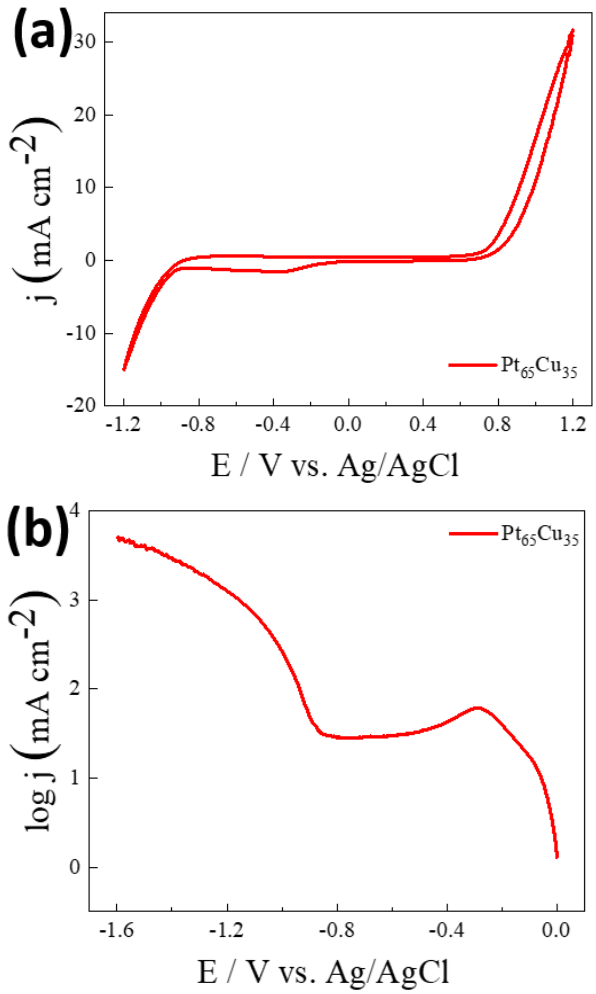

Fig. 3. (a and b) The CV and LSV curves of $Pt_{65}Cu_{35}$ NPs, respectively. All data recorded with a scan rate of 50 mV s^{-1} and 2 mV step in 1 M KOH and at room temperature.

In alkaline media, there are three steps constitute the overall mechanism of the Hydrogen Evolution Reaction (HER) in alkaline media. The kinetics of these steps, including their rate-determining factors and intermediates, play a crucial role in understanding and optimizing catalysts for efficient HER in alkaline conditions [16].

Volmer Reaction: In the first step, water molecules (H_2O) dissociate on the catalyst surface, resulting in the formation of adsorbed hydrogen ions (H*) and hydroxide ions (OH^-).

Volmer reaction:

$$Pt + H_2O + e^- \leftrightarrow PtH^* + OH^- \quad (1)$$

Heyrovsky Reaction: Following the Volmer step, a hydrogen ion (H^*) reacts with another adsorbed hydrogen ion (H^*) to form a hydrogen molecule (H_2) and regenerate the catalyst surface.

Heyrovsky reaction:

$$PtH^* + H_2O + e^- \leftrightarrow H_2 + Pt + OH^- \quad (2)$$

Tafel Reaction: Alternatively, an adsorbed hydrogen ion (H^*) can react with a hydroxide ion (OH^-) to produce water (H_2O) and free electrons (e^-) on the catalyst surface.

Tafel reaction:

$$PtH^* + PtH^* \leftrightarrow H_2 + Pt \quad (3)$$

During this procedure, hydrogen ions (H^*) interact synergistically with Pt atoms, while OH^- ions are fixed by Cu atoms, thereby resulting water dissociation [17]. The collaborative interaction between adsorbed H^* ions on Pt sites and OH^- ions on Cu sites within the alloy enhances HER activity when compared to commercially available Pt/C and Pt carbon black catalysts [18]. Notably, the (111) plane of PtCu provides enhanced dispersion and a greater abundance of active sites on the surface, thereby bolstering catalytic performance [13].

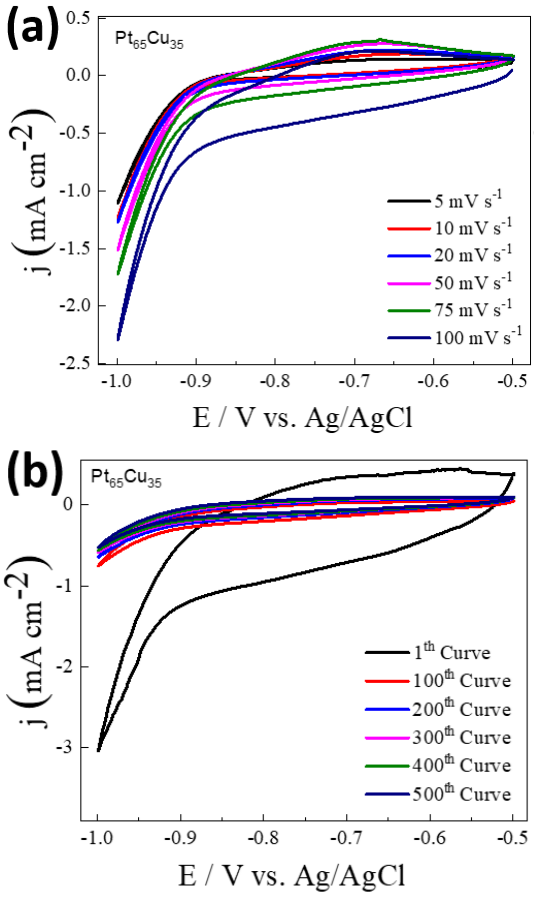

Fig. 4. The CV curves of $Pt_{65}Cu_{35}$ catalyst between -0.5 V and -1.0 V as a function of scan rates at 5 mV s^{-1}, 10 mV s^{-1}, 20 mV s^{-1}, 50 mV s^{-1}, 75 mV s^{-1} and 100 mV s^{-1}, in 1 M KOH alkaline media at room temperature. (b) The stability of

$Pt_{65}Cu_{35}$ catalyst up to 500 cycles in 1 M KOH alkaline media at room temperature.

In Fig. 4(a), the CV curves of $Pt_{65}Cu_{35}$ catalyst presented between -0.5 V and -1.0 V (vs. Ag/AgCl) as a function of scan rates at 5 mV s^{-1}, 10 mV s^{-1}, 20 mV s^{-1}, 50 mV s^{-1}, 75 mV s^{-1} and 100 mV s^{-1}, in 1 M KOH alkaline media at room temperature. At a scan rate of 100 mV s^{-1}, the $Pt_{65}Cu_{35}$ catalyst exhibited the highest recorded current density, reaching approximately 2.29 mA cm^{-2}. This elevated scan rate facilitated enhanced current flow within the electrolyte, consequently promoting increased absorption of H_2 in the negative potential region and its subsequent desorption in the positive potential region in the alkaline media. The increase in catalytic current with increasing scan rate in electrochemical measurements can be explained by the kinetics of the reaction at the electrode surface, particularly in processes involving electrocatalysis. This phenomenon is often observed in cyclic voltammetry experiments. The formula that describes the relationship between the scan rate (v) and the peak current (i_p) in cyclic voltammetry is the Randles-Sevcik equation [19]:

$$\mathrm{i}_p = \mathrm{nFAD}^{1/2}\nu^{1/2}\mathrm{C}$$

Where, i_p is the peak current, n is the number of electrons transferred in the electrochemical reaction (for hydrogen evolution reaction, n = 2), F is Faraday's constant (96,485 C/mol), A is the electrode surface area, D is the diffusion coefficient of the electroactive species in the solution and C is the concentration of the electroactive species. This equation shows that the peak current is proportional to the square root of the scan rate ($v_{1/2}$). As the scan rate increases, the rate of change of potential at the electrode surface also increases. This results in faster mass transport of reactants and products to and from the electrode surface, leading to higher currents observed in the voltammogram.

As seen in Fig. 4(b), CV curves were recorded up to 500 cycles with a potential range between -0.5 V and -1.0 V (vs. Ag/AgCl) by keeping scan rate constant, 50 mV s^{-1} in 1 M KOH alkaline media. During the 500-cycle CV test, initially, the highest current density were recorded as 3.04 mA cm^{-2} at -1 V (vs. Ag/AgCl) for the first cycle, indicative of the catalyst's initial activity. However, as the cycling progressed, the current density gradually decreased, suggesting potential changes in the catalyst's surface properties or electrode kinetics [20]. Beyond the 100th cycle, a stabilization of the current density was observed, indicating a potential equilibrium in the catalytic process or the establishment of a steady-state regime. This stabilization implies a level of durability and consistency in the catalyst's performance over prolonged cycling, offering insights into its long-term viability for practical applications requiring sustained catalytic activity [21].

4. Conclusion

In conclusion, the structural characterization of $Pt_{65}Cu_{35}$ alloy NPs through XRD analysis revealed crucial insights into their crystalline properties. The presence of characteristic Miller indices of (111), (200), (220), (311), and (222) facets confirmed the face-centered-cubic (fcc) Pt_3Cu_1 phase, indicative of a well-defined crystal structure. Further analysis determined a lattice parameter of a=b=c=3.923 Å, signifying a uniform crystal lattice. Additionally, assessment of crystallite size and microstrain highlighted the influence of PtCu alloy formation on the structural defects and grain boundaries within the NPs. Moreover, SEM-EDS confirmed the elemental composition of $Pt_{65}Cu_{35}$ NPs, corroborating the XRD findings. The spherical morphology of the NPs, attributed to the influence of PVP molecules, was evident in the SEM images, underscoring the importance of synthesis conditions in shaping nanostructures. Furthermore, the stoichiometric analysis revealed a PtCu composition of 65% Pt and 35% Cu, aligning with the XRD and EDS data. The electrocatalytic performance of the $Pt_{65}Cu_{35}$ catalyst for the HER was thoroughly investigated, revealing promising results. The CV and LSV analyses depicted Pt-H formation and H_2 gas evolution, with a maximum current density of 1.52 mA cm^{-2} observed at -0.37 V. Additionally, CV curves recorded over 500 cycles further elucidated the catalyst's behavior, with the initial cycle exhibiting the highest current density of 3.04 mA cm-2 at -1 V. However, a gradual decrease in current density was observed over subsequent cycles, potentially indicating changes in surface properties or electrode kinetics. Notably, beyond the 100th cycle, a stabilization of current density was observed, suggesting the establishment of a steady-state regime. These findings underscore the excellent electrocatalytic performance of the $Pt_{65}Cu_{35}$ catalyst, highlighting its potential for various applications in electrochemical processes. Further research could focus on elucidating the underlying mechanisms governing the observed cyclic behavior, facilitating the optimization of catalyst design for enhanced performance and durability in practical applications.

References

[1] Li Y, Wang H, Priest C, Li S, Xu P, Wu G. Advanced Electrocatalysis for Energy and Environmental Sustainability via Water and Nitrogen Reactions. 2021;33:2000381.

[2] Yaashikaa PR, Kumar PS. Fabrication and characterization of magnetic nanomaterials for the removal

of toxic pollutants from water environment: A review. Chemosphere. 2022;303:135067.

[3] Sharma R, Wang Y, Li F, Chamier J, Andersen SM. Particle Size-Controlled Growth of Carbon-Supported Platinum Nanoparticles (Pt/C) through Water-Assisted Polyol Synthesis. ACS Omega. 2019;4:15711-20.

[4] Zhang H, Guo X, Liu W, Wu D, Cao D, Cheng D. Regulating surface composition of platinum-copper nanotubes for enhanced hydrogen evolution reaction in all pH values. J Colloid Interface Sci. 2023;629:53-62.

[5] Zheng J, Sheng W, Zhuang Z, Xu B, Yan Y. Universal dependence of hydrogen oxidation and evolution reaction activity of platinum-group metals on pH and hydrogen binding energy. 2016;2:e1501602.

[6] Cowley A. Johnson Matthey PGM market report May 2020. USA2020.

[7] Marini S, Salvi P, Nelli P, Pesenti R, Villa M, Berrettoni M, et al. Advanced alkaline water electrolysis. Electrochim Acta. 2012;82:384-91.

[8] Zhu Z, Zhai Y, Dong S. Facial Synthesis of PtM (M = Fe, Co, Cu, Ni) Bimetallic Alloy Nanosponges and Their Enhanced Catalysis for Oxygen Reduction Reaction. ACS Appl Mater Interfaces. 2014;6:16721-6.

[9] Abdelsayed V, Glaspell G, Nguyen M, Howe JM, Samy El-Shall M. Laser synthesis of bimetallic nanoalloys in the vapor and liquid phases and the magnetic properties of PdM and PtM nanoparticles (M = Fe, Co and Ni). Faraday Discuss. 2008;138:163-80.

[10] Yan W, Zhang D, Zhang Q, Sun Y, Zhang S, Du F, et al. Synthesis of PtCu–based nanocatalysts: Fundamentals and emerging challenges in energy conversion. J Energy Chem. 2022;64:583-606.

[11] Chen G, Shan H, Li Y, Bao H, Hu T, Zhang L, et al. Hollow PtCu nanoparticles encapsulated into a carbon shell via mild annealing of Cu metal–organic frameworks. J Mater Chem A. 2020;8:10337-45.

[12] Fang D, Wan L, Jiang Q, Zhang H, Tang X, Qin X, et al. Wavy PtCu alloy nanowire networks with abundant surface defects enhanced oxygen reduction reaction. Nano Res. 2019;12:2766-73.

[13] Zhang X-F, Wang A-J, Zhang L, Yuan J, Li Z, Feng J-J. Solvothermal Synthesis of Monodisperse PtCu Dodecahedral Nanoframes with Enhanced Catalytic Activity and Durability for Hydrogen Evolution Reaction. ACS Applied Energy Materials. 2018;1:5054-61.

[14] Kaya D, Demiroglu I, Isik IB, Isik HH, Çetin SK, Sevik C, et al. Highly active bimetallic Pt–Cu nanoparticles for the electrocatalysis of hydrogen evolution reactions: Experimental and theoretical insight. Int J Hydrogen Energy. 2023.

[15] Tong YY. Polyvinylpyrrolidone (pvp) for enhancing the activity and stability of platinum-based electrocatalysts. Google Patents; 2015.

[16] Tian X, Zhao P, Sheng W. Hydrogen Evolution and Oxidation: Mechanistic Studies and Material Advances. 2019;31:1808066.

[17] Cao Z, Chen Q, Zhang J, Li H, Jiang Y, Shen S, et al. Platinum-nickel alloy excavated nano-multipods with hexagonal close-packed structure and superior activity towards hydrogen evolution reaction. Nature communications. 2017;8:15131-.

[18] Zheng Y, Jiao Y, Jaroniec M, Qiao SZ. Advancing the electrochemistry of the hydrogen-evolution reaction through combining experiment and theory. Angewandte Chemie (International ed in English). 2015;54:52-65.

[19] Abdi Z, Vandichel M, Sologubenko AS, Willinger M-G, Shen J-R, Allakhverdiev SI, et al. The importance of identifying the true catalyst when using Randles-Sevcik equation to calculate turnover frequency. Int J Hydrogen Energy. 2021;46:37774-81.

[20] Jeyabharathi C, Hodnik N, Baldizzone C, Meier JC, Heggen M, Phani KLN, et al. Time Evolution of the Stability and Oxygen Reduction Reaction Activity of PtCu/C Nanoparticles. ChemCatChem. 2013;5:2627-35.

[21] Hodnik N, Jeyabharathi C, Meier JC, Kostka A, Phani KL, Rečnik A, et al. Effect of ordering of PtCu3 nanoparticle structure on the activity and stability for the oxygen reduction reaction. Phys Chem Chem Phys. 2014;16:13610-5.